CHEMISTRY
AN ASIAN JOURNAL
www.chemasianj.org

Accepted Article

Title: Near Infrared BODIPY for bioimaging and photothermal therapy

Authors: yang liu, nan song, li chen, shi liu, and zhigang xie

To be cited as: *Chem. Asian J.* 10.1002/asia.201701727

Link to VoR: http://dx.doi.org/10.1002/asia.201701727

A Journal of

ACES
Asian Chemical Editorial Society

A sister journal of **Angewandte Chemie** and **Chemistry – A European Journal**

WILEY-VCH

10.1002/asia.201701727

WILEY-VCH

Near Infrared BODIPY for bioimaging and photothermal therapy

Yang Liu,[a] Nan Song, [a] Li Chen, *[a] Shi Liu*[b] and Zhigang Xie[b]

Abstract: It is challenging to develop robust photothermal agents with near-infrared (NIR) imaging simultaneously. In this work, a new photothermal agent was designed and synthesized based on aza-boron-dipyrromethene (aza-BDP). The aza-BDP possesses excellent photostability and higher photothermal conversion efficiency (50%) under NIR laser irradiation. When the photothermal effects were utilized for tumor inhibition, long term stable fluorescence was observed in living animals. The photothermal treatment can efficiently suppress the tumor growth, which was evidenced by in vitro and in vivo experiments. Meanwhile, the NIR emission can be detected by imaging system and achieved therapeutic self-monitoring under the guidance of NIR imaging. This work highlights the potential of rational design of molecular structures for desired functional and applications.

Photothermal therapy (PTT) has great potential for cancer treatment and possesses many advantages over conventional treatments, such as low toxicity, high selectivity, minimal invasiveness.[1] The photothermal agents upon irradiation can convert the photon energy into heat, which can kill the tumor cells.[2] The absorbance of most current photothermal agents used for PTT focus on NIR region, which is known as the transparent window for deep tissue penetration. So far, the photothermal agents, such as the gold nanoparticles and rods,[3] metal-organic structures,[4] belong to inorganic materials and have been used for PTT. Comparing with inorganic counterpart, organic substances possess some superiorities of good biocompatibility and potential biodegradability. Therefore, the organic molecules, such as porphyrin derivatives[2k,5] and cyanine dye,[6] were widely developed for PTT. However, the relative low stability of cyanines dyes and complicated synthesis of porphyrin derivatives with NIR absorption spurs new exploring in organic photothermal agents.

Compared with the porphyrin and cyanine dye, the aza-boron-dipyrromethene (aza-BDP) possesses tunable NIR absorption, high molar absorption coefficient and good photostability.[7] Up to now, most of aza-BDP were used for photodynamic therapy, [8] little attention was paid on photothermal therapy. In the previous work, azaBDP with the photothermal activity is realized through introducing the heavy atom (such as iodine) or polymerization, which could lead to singlet-to-triplet transition and nonradiative decay upon light irradiation.[9] However, the generated photothermal effect is at the expense of losing fluorescence for bioimaging. Hence, it is imperative to develop fluorescent azaBDP molecule with photothermal activity.

In this work, we designed and synthesized a new fluorescent azaBDP molecule, which possesses excellent photothermal effect and fluorescence imaging in the absence of the heavy atom. The photothermal property of azaBDP was studied in vitro as well as its phototoxicity against Murine colon cancer (CT26) and Human cervical carcinoma (HeLa) cells line. In vitro and in vivo experiments further demonstrated the azaBDP molecule can generate heat, which greatly inhibited tumor growth by PTT under the guidance of NIR imaging and achieve therapeutic self-monitoring in the NIR region.

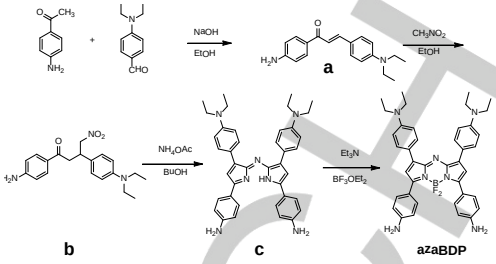

Scheme 1. The synthesis procedure of the target compound azaBDP

The detailed synthetic route of azaBDP was shown in Scheme 1. The chaltone (a) was synthesized by aldol condensation reaction in mild condition, and structure was validated unambiguously by ^{1}H NMR as shown in Figure S1(a). The double peaks at 7.75 and 7.33 ppm in the 1H NMR spectrum ascribed to the vinylic protons resonating explicitly indicated the compound structure. The mediated product b was obtained by Michael addition reaction. The compound b and c directly used for the next step reaction. Target molecule azaBDP was successfully synthesized by above three steps, and structure was confirmed by ^{1}H NMR and ESI-MS analysis. As shown in Figure S1(b), the integration ratios of these peaks in the ^{1}H NMR spectrum agreed well with those of theoretical values. The signal of m/z at 669.4 (Figure S2) was close to the theoretical molecular weight. Photophysical properties were investigated by UV-Vis absorbance and emission spectra. As shown in Figure 1a, the target compound in organic solvent (THF) exhibited an intense absorption peak at 781 nm, a moderated peak at around 612 nm and a weak peak at 373 nm. The maximum emission in THF is at 830 nm. The absolute quantum field is 0.9 % in DMF.

The photothermal property was studied in DMF with various laser power intensity and concentrations. With the increase of the laser power from 1 W cm^{-2} to 2 W cm^{-2} (35 μg mL^{-1}, 808 nm, 5 min), temperature reached to 74.5 ^{o}C from 25.4 ^{o}C, which is dependent to the laser power intensity (Figure 1b). The photothermal effect of azaBDP also performed the dependence

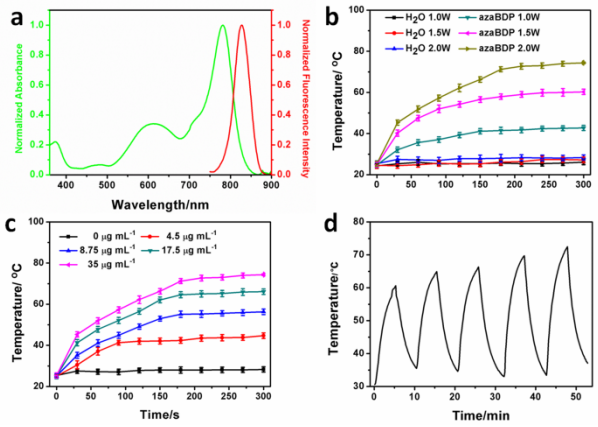

Figure 1. The basic photophysical and photothermal property study of azaBDP in vitro: a) The Normalized absorbance and fluorescence spectra (λ_{ex} = 750 nm) in THF. b) Fixed concentrations (35 μg mL^{-1}) with various irradiation intensities along with time in DMF. c) Temperature rise curves of azaBDP at various concentrations under irradiation (808 nm, 2 W cm^{-2}) in DMF. d) Heating reproducibility stability of azaBDP (808 nm, 2 W cm^{-2}, 35 μg mL^{-1}) in DMF.

[a] Yang Liu, Nan Song, Li Chen
Department of Chemistry
Northeast Normal University
Changchun 130024 (P. R. China)
E-mail: chenl686@nenu.edu.cn
[b] Shi Liu, Zhigang Xie
State key of Polymer Physics and Chemistry
Changchun Institute of Applied Chemistry
Chinese Academy of Science
Changchun 130022 (P. R. China)
E-mail: liushi@ciac.ac.cn

Supporting information for this article is given via a link at the end of the document.

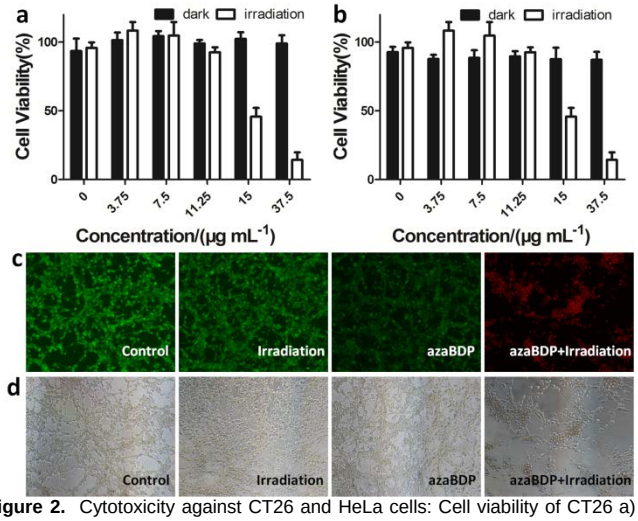

Figure 2. Cytotoxicity against CT26 and HeLa cells: Cell viability of CT26 a) and HeLa b) cells incubated with azaBDP for 24h at the various concentration after irradiation (1 W cm^{-2}) for 5 min by 808 nm laser at 37°C .c) Fluorescence images of calcein AM (green, live cells) and propidium iodide (red, dead cells) co-stained. d) The bright field photos of CT26 cells (c and d: CT26 cells incubated for 24 h with the azaBDP at the concentration of 37.5 μg mL^{-1} after irradiation (1 W cm^{-2}) for 5 min by 808 nm laser at 37 ^{o}C).

of concentration as shown in Figure 1c. The maximum temperature increasing is to 74.5 ^{o}C at the concentration of 35 μg mL^{-1} upon the irradiation for 5 min. And the temperature rising curves in PH 5.0 and 7.4 are basically consistent at the concentration of 35 μg mL^{-1} upon the irradiation for 5 min. (Figure S3). For quantative evaluating the photothermal effect of the azaBDP, the photothermal conversion experiment was carried out (Figure S4). The photothermal conversion efficiency is 55 % according to previous method, which is higher than most of reported value of photothermal agents[9,11] and enough for PTT. The photothermal stability of azaBDP was investigated by multiple cycles of laser irradiation (Figure 1d). The maximum temperature increasing under continuous laser irradiation for different cycles slightly increased after heating cooling cycles. Major cause is the evaporation of solvent leading to the concentration of azaBDP increasing.

The cell uptake and imaging of azaBDP was investigated in HeLa cells by confocal lasser scanning microscopy (CLSM) and flow cytometry. The 4',6-diamidino-2-phenyl-indole (DAPI) was used to stain the cellular nuclei. As shown in Figure S5a, the azaBDP was not observed in the cellular nuclei. The azaBDP located abundantly in the cytoplasm of the HeLa cells and the fluorescence intensity significantly enhanced with time increasing from 0.5 h to 2 h indicating the time-dependent endocytosis and the enhanced cellular uptake of azaBDP was also confirmed by flow cytometry (Figure S5b).

In order to investigate the darktoxicity and phototoxicity of azaBDP to CT26 and HeLa cells, 3-(4,5-dimethylthiazol-2-yl)-2,5-diphenyl-tetrazol-ium bromide (MTT) assay was carried out at various concentrations (0 - 37.5 μg mL^{-1}) in the presence or absence of 808 nm laser irradiation (1 W cm^{-2}, 5 min). Figure S6 shows the cell viability of CT26 and HeLa cells after 24 h incubated with azaBDP at different concentrations. It can be seen that all the cell viability are more than 80 %, which suggests the azaBDP possess good biocompatibility. As shown in Figure 2a, after the CT26 cells incubated with azaBDP for 24 h, the cell viability significantly decreased under irradiation in a dose-dependent manner with a half maximal inhibitory concentration (IC50) of 15.5 μg mL^{-1}. Similar results were observed for HeLa cells with IC50 of 18.3 μg mL^{-1} upon laser irradiation in Fig. 2b. Such good biocompatibility and high phototoxicity of azaBDP make them desirable for PTT.

To further demonstrate that cell apoptosis and necrosis is triggered by irradiation, the CT26 cells were selected for the live/dead staining and stained with calcein-AM and propidium iodide (PI) to differentiate live (green) and dead/late apoptotic (red) cells, respectively. Figure 2c shows the cells without irradiation were in healthy condition with strong green fluorescence. Meanwhile, most of the cells under irradiation or only treated with azaBDP in the dark were alive with plentiful green fluorescence. Almost all cells treated with azaBDP and laser irradiation were dead with strong red fluorescence. Simultaneously, CT26 cells were pretreated like the live/dead staining method and the bright field photos of CT26 cells were obtained. As shown in Figure 2d, almost all the CT26 cells were in normal state after treated with irradiation and azaBDP. When the cells were treated with azaBDP under irradiation, the cellular outline was broken. These results indicated that the azaBDP under irradiation could generate heat and evoke irreversible cell damage.

The real-time dynamic accumulation a bearing CT26 in back were imaged at different time points after intratumoral and intravenous injection the azaBDP as shown in Figure 3. After intratumoral injection, the fluorescence signs concentrated on the center of tumor in one hour. With time going on, the fluorescence intensity gradually increased and diffused to peripheral tissue at 7d. Finally, the fluorescence gradually became weaker due to the metabolism. Figure 3b shows the images of mouse with intravenous injection. The fluorescence could be seen throughout whole body of mice in 30 mins. The accumulation of zazBDP was observed in tumor at 12 h. With the passage of time, the fluorescence gradually became stronger and the fluorescence in other parts of mouse gradually became weaker and disappeared in 10 days. Interesting, the fluorescence in tumor did not weaken even after 13 d. This implies the azaBDP could effectively gathering in tumor and possibly provide the guidance for the PTT.

Next, we studied the biodistribution of azaBDP by collecting the fluorescence in the tumor and major organs excised from the mice treated by tail intravenous injection. Figure 3c, d shows the images of major organ and tumor excised in bright field and NIR light after 24 h. The azaBDP mainly distributed in tumor and normal organs with the highest accumulations in the spleen, lung and liver, followed by tumor and kidney. After 48h (Figure 3e,f) , the distribution of azaBDP was similar to the result at 24 h. The higher fluorescence in the liver and spleen suggested that azaBDP were mainly eliminated by macrophage cells of the liver and spleen. In order to illustrate the long term photosensitizer for fluorescence imaging, the pharmacokinetics experiment was conducted. As shown in Figure S7a, the azaBDP is mainly concentrated in tumor and liver and the fluorescence intensity gradually decreased within 13 days. It's worth noting that clearance rate of azaBDP in liver is much faster than that in tumor from the 6th day. On day13, the fluorescence intensity in

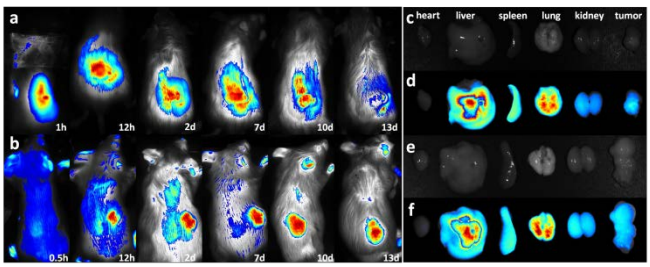

Figure 3. In vivo imaging study of azaBDP: In vivo NIR fluorescence images of CT26 tumor bearing Balb/c mouse at different time points injected intratumor a) and tail-vain b) post-injection of azaBDP. Ex in vivo bright field photos of mouse being administrated with azaBDP after 24 h c) and 48 h e). Ex in vivo NIR images of mouse being administrated with azaBDP after 24 h d) and 48h f). Excitation wavelength: 704 nm; images were obtained through a 750 nm filter.

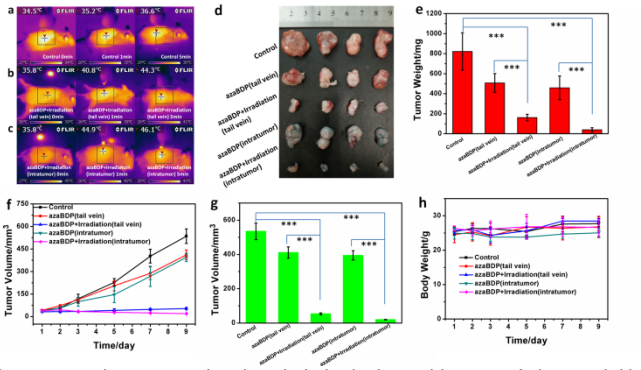

Figure 4. In vivo PTT study: The whole-body thermal images of a) control, b) injected tail vein and c) injected intratumor of azaBDP solution (0.1 mL, 2 mg mL^{-1}, dissolved by Vcaster oil: Vethanol: VPBS =1:1:2). d) Representative photos of tumor isolated. e) Quantitative analysis of tumor weight each group. f) Tumor grows rates of each group after different treatments. g) Quantitative analysis of eventual tumor volume each group at 9 d. h) Changes in body weight of mice with CT26 tumors upon various treatments. Statistical significance: ***P < 0.001.

tumor is the strongest among all organs, suggesting that azaBDP may be a long term photosensitizer for fluorescence imaging of tumor. We also detected the fluorescence of plasma in different time. As shown in Figure S8b, the fluorescence intensity gradually decreased as time goes on and the azaBDP has basically been eliminated in 9 days and the semiquantitative average signal was shown in Figure S8c.

In order to study the PTT effect of the azaBDP, the CT26 xenograft models were established by subcutaneous inoculation at the back of Balb/c. These mice were randomly divided into five groups and subjected five different treatments: group 1, introtumor injection solution 100 μL (caster oil: ethanol: PBS, V/V/V=1:1:2) with irradiation as control; group 2, tail-vein injection of azaBDP; group 3, tail-vein injection of azaBDP and laser irradiation; group 4, intratumor injection of azaBDP; group 5, intratumor injection of azaBDP and laser irradiation. The thermal imaging was used to monitor the changes of temperature in vivo using an infrared red camera. Figure 4a, 4b and 4c respectively shows the thermal images treated with irradiation (group 1), intravenous injection under irradiation (group 3) and intratumor injection under irradiation (group 5). The temperature of group 1 only increased 2.1 ^{o}C in 5 min as a control (Figure 4a). The group 3 was irradiated after injection 12 h because of the accumulation of azaBDP in tumor under the guidance of NIR imaging (Figure 4b). The temperature of group 3 gradually increased to 44.3 ^{o}C in 5 min. The temperature of group 5 increased to 44.9 ^{o}C in 1 min and reached to 46.1 ^{o}C in 5 min under irradiation (1.0 W cm^{-2}) (Figure 4c). The tumor size dissected from the intratumor injection under irradiation group was smallest compared with other 4 groups. For the intravenous injection under irradiation group, the tumor size is bigger than intratumor injection under irradiation but the tumor inhibition is obvious (Figure 4d,e). Especially, the tumors treated with azaBDP and irradiation showed complete tumor regression compared to the control, intratumor injection and intravenous injection groups after 9 d. Tumor suppress efficiency is about 96 % for intratumor injection and 89 % for intravenous injection (Figure 4f,g). The body weight of mouse was tested all through and increased gradually. No significant toxic effects were observed after the photothermal treatment compared with control groups (Figure 4h). Figure S9 shows the H&E staining of the major organs (heart, liver, spleen, lung, and kidney). Compared with the control group (Figure S9a), no obvious histological alterations can be identified for injected with azaBDP (Figure S9b), further confirming the in vivo biocompatibility.

In summary, we successfully designed and synthesised a novel aza-BODIPY photothermal agents (azaBDP) with high photothermal conversion efficiency, high photo stability and NIR imaging. The NIR imaging enable locating tumors, real-time monitoring of the photosensitizer distribution and its accumulation and guiding the PTT. The thermal imaging can real-time monitoring of the temperature change at the tumor site in order to determine the optimal irradiation protocol. In vitro and in vivo experiments indicates demonstrated the azaBDP is effective for PTT. We believe that the azaBDP are a promising imaging-guided photothermal agent for PTT.

Experimental Section

Materials

Solvents and reagents were purchased commercially as reagent grade and used as received unless otherwise mentioned. Dichloromethane (CH_2Cl_2) was distilled over calcium hydride. The solvents used for spectroscopic measurements were of HPLC grade.

Instruments

^{1}H-NMR spectra were recorded on a Bruker NMR 400 DRX Spectrometer using $CDCl_3$ as solvent. UV-Vis absorption and emission measurement were carried on by using a Shimadzu UV-2450 PC UV-Vis Spectrophotometer and a PerkinElmer LS-55 Fluorescence Spectrophotometer, respectively. Electrospray Ionization (ESI) mass spectra were obtained on a Finnigan LCQ quadrupole ion trap mass spectrometer.Confocal laser scanning microscopy (CLSM) images were taken using a Zeiss LSM 700 (Zurich, Switzerland). Fluorescence quantum efficiency was obtained on a Hamamatsu Absolute PL Quantum Yield Measurement System C9920-02.

Cell imaging and flow cytometry

The Human cervical carcinoma (HeLa) cells were cultured in Dulbecco's modified Eagle's medium (DMEM, GIBCO) containing 10% fetal bovine serum (FBS, GIBCO), 100 μg mL^{-1} streptomycin and 100 U mL^{-1} penicillin at 37 ^{o}C in a humidified incubator containing 5% CO_2 and 95% air. After the HeLa cells were cultured for 24 h, the azaBDP (5μg mL^{-1}) was added and the cells were cultured for another 0.5 and 2 hours. The cells nuclei were stained by DAPI. The result of flow cytometry was obtained by flow cytometer according to the treatment of cell imaging.

Calcein-AM/PI Test

To visually demonstrate the efficiency of azaBDP in photodythermal therapy, the CT26 cells were stained with propidium iodide and calcein-AM to identify dead (red) and live (green) cells, respectively. The control and drug-treated cells were incubated at 37 °C for 24 h in a humidified atmosphere containing 5% CO_2. Then, all dishes of cells were irradiated for 30 min with a 808 nm laser at an intensity of 1 W/cm^2 . Then, the cells were further incubated at 37 °C for another 24 h. After staining with calcein-AM/PI for 40 min and washing with PBS, the two samples of cells were imaged with a fluorescence microscope.

MTT assay

HeLa and CT26 cells harvested were seeded in 96-well plates with a density of 105 cells in every well and cultured in DMEM for 24 h. The medium was replaced by azaBDP at a final concentration respectively. After 4h at the various concentration upon irradiation (1 W cm^{-2}) for 5 min by 808 nm laser at 37°C and cultured another 24 h, and then the medium was replaced by the new medium with the MTT and cultured another 4 h. The medium was removed and followed the addition of 150 μL of DMSO. The absorbance wavelength was set at 490 nm to measure the results by a microplate reader.

In Vivo Fluorescence Imaging and tumor inhibition

All animal experiments were performed complying with the NIH guidelines for the care and use of laboratory animals. The xenograft tumors were established by subcutaneously injecting CT26 cells into the back of Kunming mice. After tumors of 4-5 mm in diameter were palpable, tumor images of mice were acquired respectively by intratumoral injection and tail vein injection of 100 μL of azaBDP at a concentration of 2 mg mL^{-1}. All images were analyzed and collected at the indicated time points with an in vivo imaging system (Maestro 500FL in vivo optical imaging system). For the PTT, these mice bearing CT26 were randomly divided into 5 groups and were subjected five different treatments: group 1, introtumor injection solution 100 μL (caster oil: ethanol:

PBS,V/V/V==1:1:2); group 2, tail-vein injection 100 μL solution of azaBDP at a concentration of 2 mg mL^{-1} only; group 3, tail-vein injection 100 μL of azaBDP at a concentration of 2 mg mL^{-1} with NIR light exposure; group 4, intratumor injection 100 μL solution of azaBDP at a concentration of 2 mg mL^{-1}; group 5, intratumor injection 100 μL solution of azaBDP at a concentration of 2 mg mL^{-1} with NIR light exposure. Each group contained four mice. Injected 12 h later, laser was performed on groups3, 5, by irradiating the tumor region with a 808 nm (at 1W cm^{-2}) for 10 min. Different treatment groups were monitored by measuring the tumor size using a Vernier caliper for 9 d after the PTT treatment. Tumor size = width × width × length/ 2.

Histological examination analysis
The hematoxylin and eosin (H&E) staining assays were carried out to stain tissue slices. The major organs (heart, lung, liver, spleen and kidney) were stained with H&E for histological examination.

Synthesis
The synthesis of compound a. p-Diethylaminobenzaldehyde (3,54 g, 20 mmol) and p-Aminoacetophenone (2.7 g, 20 mmol) were dissolved in ethanol (20 mL), 10% NaOH (10 mL) was slowly dropped in the above solution, the reaction mixture was stirred at room temperature over night and cold trap dry solvents. The residue was dissolved in CH_2Cl_2 and washed with water and brine. The organic layer was dried with anhydrous Na_2SO_4. The solvent was removed under reduced pressure, and the residue was purified by column chromatography on silica gel eluting with EtOAC/petroleum ether (1/1) to give the product afford the yellow compound (2 g, 34%). ^{1}H NMR (400 MHz, CDCl3) δ 7.94 – 7.88 (m, 2H), 7.75 (d, J = 15.4 Hz, 1H), 7.51 (d, J = 8.9 Hz, 2H), 7.33 (d, J = 15.4 Hz, 1H), 6.72 – 6.61 (m, 4H), 4.12 (s, 2H), 3.40 (q, J = 7.1 Hz, 4H), 1.20 (t, J = 7.1 Hz, 6H).

The synthesis of compound b. A solution of chalcone a (1.19 g, 4 mmol), nitromethanol (4.88 g, 80 mmol) and NaOH (32 mg, 0.8 mmol) in ethanol (10 mL) was heated at 60 °C for 12 h. After cooling to room temperature, the solvent was removed in vacuo and the oily residue obtained was dissolved in ethyl acetate and washed with water. The combined organic layer was washed with brine, dried over sodium sulfate, and concentrated to give the target compound as a yellow oily residue (1.12 g, 78%). This product was used in the next without further purification.

The synthesis of compound c. The compound b (1.12g, 3 mmol) and ammonium acetate (8.08 g, 105 mmol) were poured into a 50 mL round-bottomed flask, then the butanol (30 mL) was added and heated under reflux for 24 h. After cooling to room temperature, the formed precipitate was filtered, washed with cold ethanol and diethyl ether to givea blue-black solid product (470 mg, 45%). This product was used in the next without further purification.

The synthesis of compound azaBDP. Compound c (124 mg, 0.2 mmol) was dissolved in dry CH_2Cl_2 (40 mL) in the dark under Ar, and Et_3N (11 mL, 60 mmol) was then added. After the solution was stirred for 30 min, BF_3OEt_2 (7.4 mL, 60 mmol) was added, which was stirred at room temperature for 24 h. The reaction mixture was washed with water and brine. The organic layer was dried with anhydrous Na_2SO_4. The solvent was removed under reduced pressure, and the residue was purified by column chromatography on silica gel eluting with CH_2Cl_2/EtOAc (v/v=1/1) to give the product azaBDP as blue-purple solid (85 mg, 63%). ^{1}H NMR (400 MHz, CDCl3) δ 8.05 (d, J = 8.8 Hz, 4H), 7.96 (d, J = 8.5 Hz, 4H), 6.81 (s, 2H), 6.72 (dd, J = 8.5, 4.5 Hz, 8H), 3.98 (s, 4H), 3.44 (q, J = 6.9 Hz, 8H), 1.23 (t, J = 7.0 Hz, 12H)..

Acknowledgements

This work was supported by the National Natural Science Foundation of China (Project. No. 51522307).

Keywords: azaBDP • NIR-imaging • photothermal therapy

[1] a) L. Cheng, C. Wang, L. Feng, K. Yang, Z. Liu, *Chem. Rev.* **2014**, 114, 10869-10939; b) H. S. Jung, J. H. Lee, K. Kim, S. Koo, P. Verwilst, J. L. Sessler, C. Kang, J. S. Kim, *J. Am. Chem. Soc.* **2017**, 139, 9972-9978; c) R. Lv, C. Zhong, R. Li, P. Yang, F. He, S. Gai, Z. Hou, G. Yang, J. Lin, *Chem. Mater.* **2015**, 27, 1751-1763; d) Q. Tang, W. Xiao, C. Huang, W. Si, J. Shao, W. Huang, P. Chen, Q. Zhang, X. Dong, *Chem. Mater.* **2017**, 29, 5216-5224; e) M. Zheng, Y. Li, S. Liu, W. Wang, Z. Xie, X. Jing, *ACS Appl. Mater. Interfaces* **2016**, 8, 23533-23541; f) S. B. Kim, T. H. Lee, I. Yoon, Y. K. Shim, W. K. Lee, *Chem. - Asian J.* **2015**, 10, 563-567.

[2] a) M. Abbas, Q. Zou, S. Li, X. Yan, *Adv. Mater.* **2017**, 29; b) Y. Cai, P. Liang, Q. Tang, X. Yang, W. Si, W. Huang, Q. Zhang, X. Dong, *ACS nano* **2017**, 11, 1054-1063; c) X. Ding, J. Liu, J. Li, F. Wang, Y. Wang, S. Song, H. Zhang, *Chem. Sci.* **2016**, 7, 6695-6700; d) P. Huang, J. Lin, W. Li, P. Rong, Z. Wang, S. Wang, X. Wang, X. Sun, M. Aronova, G. Niu, R. D. Leapman, Z. Nie, X. Chen, *Angew. Chem., Int. Ed. Engl.* **2013**, 52, 13958-13964; e) X. Liang, L. Fang, X. Li, X. Zhang, F. Wang, *Biomaterials* **2017**, 132, 72-84; f) L. Pan, J. Liu, J. Shi, *ACS Appl. Mater. Interfaces* **2017**, 9, 15952-15961; g) D. Yin, X. Li, Y. Ma, Z. Liu, *Chem. Commun.* **2017**, 53, 6716-6719; h) Z. Yu, M. Wang, W. Pan, H. Wang, N. Li, B. Tang, *Chem. Sci.* **2017**, 8, 4896-4903; i) X. Zhang, X. Nan, W. Shi, Y. Sun, H. Su, Y. He, X. Liu, Z. Zhang, D. Ge, *Nanotechnology* **2017**, 28, 295102; j) F. Zhao, X. Li, J. Li, Y. Dou, L. Wang, M. Wu, Y. Liu, J. Chang, X. Zhang, *J. Mater. Chem. B* **2017**, 5, 2145-2151; k) Q. Zou, M. Abbas, L. Zhao, S. Li, G. Shen, X. Yan, *J. Am. Chem. Soc.* **2017**, 139, 1921-1927. l) Z. Liu, L. Chan, L. Chen, Y. Bai, T. Chen, *Chem. - Asian J.* **2016**, 11, 3032-3039; m) H. X. Zhao, H. Wang, Q. Zou, S. K. Sun, C. Yu, X. Zhang, Y. Y. Fu, *Chem. - Asian J.* **2016**, 11, 2458-2469.

[3] a) X. Cheng, R. Sun, L. Yin, Z. Chai, H. Shi, M. Gao, *Adv. Mater.* **2017**, 29; b) Z. Li, H. Huang, S. Tang, Y. Li, X. F. Yu, H. Wang, P. Li, Z. Sun, H. Zhang, C. Liu, P. K. Chu, *Biomaterials* **2016**, 74, 144-154; c) A. Neshastehriz, M. Tabei, S. Maleki, S. Eynali, A. Shakeri-Zadeh, *J. Photochem. Photobiol., B* **2017**, 172, 52-60; d) B. K. Wang, X. F. Yu, J. H. Wang, Z. B. Li, P. H. Li, H. Wang, L. Song, P. K. Chu, C. Li, *Biomaterials* **2016**, 78, 27-39; e) J. Zhang, J. Li, N. Kawazoe, G. Chen, *J. Mater. Chem. B* **2017**, 5, 245-253.

[4] a) W. Wang, L. Wang, Y. Li, S. Liu, Z. Xie, X. Jing, *Adv. Mater.* **2016**, 28, 9320-9325; b) D. Yang, G. Yang, S. Gai, F. He, G. An, Y. Dai, R. Lv, P. Yang, *Nanoscale* **2015**, 7, 19568-19578; c) Y. Yang, J. Liu, C. Liang, L. Feng, T. Fu, Z. Dong, Y. Chao, Y. Li, G. Lu, M. Chen, Z. Liu, *ACS nano* **2016**, 10, 2774-2781; d) Y. D. Zhu, S. P. Chen, H. Zhao, Y. Yang, X. Q. Chen, J. Sun, H. S. Fan, X. D. Zhang, *ACS Appl. Mater. Interfaces* **2016**, 8, 34209-34217.

[5] a) B. Guo, G. Feng, P. N. Manghnani, X. Cai, J. Liu, W. Wu, S. Xu, X. Cheng, C. Teh, B. Liu, *Small* **2016**, 12, 6243-6254; b) C. S. Jin, J. F. Lovell, J. Chen, G. Zheng, *ACS nano* **2013**, 7, 2541-2550; c) S. Su, Y. Ding, Y. Li, Y. Wu, G. Nie, *Biomaterials* **2016**, 80, 169-178.

[6] a) J. Chen, Z. Sheng, P. Li, M. Wu, N. Zhang, X. F. Yu, Y. Wang, D. Hu, H. Zheng, G. P. Wang, *Nanoscale* **2017**; b) K. Deng, Z. Hou, X. Deng, P. Yang, C. Li, J. Lin, *Adv. Funct. Mater.* **2015**, 25, 7280-7290; c) B. Liu, C. Li, B. Xing, P. Yang, J. Lin, *J. Mater. Chem. B* **2016**, 4, 4884-4894; d) X.-H. Wang, H.-S. Peng, W. Yang, Z.-D. Ren, X.-M. Liu, Y.-A. Liu, *J. Mater. Chem. B* **2017**, 5, 1856-1862; e) J. Zhang, S. Liu, X. Hu, Z. Xie, X. Jing, *ACS Biomater. Sci. Eng.* **2016**, 2, 1942-1950.

[7] a) Y. Gawale, N. Adarsh, S. K. Kalva, J. Joseph, M. Pramanik, D. Ramaiah, N. Sekar, *Chem. - Eur. J.* **2017**, 23, 6570-6578; b) K. Miki, A. Enomoto, T. Inoue, T. Nabeshima, S. Saino, S. Shimizu, H. Matsuoka, K. Ohe, *Biomacromolecules* **2017**, 18, 249-256; c) Y. Ni, J. Wu, *Org. Biomol. Chem.* **2014**, 12, 3774-3791.

[8] a) N. Adarsh, R. R. Avirah, D. Ramaiah, *Org. Lett.* **2010**, 12, 5720-5723; b) X.-D. Jiang, D. Xi, B. Le Guennic, J. Guan, D. Jacquemin, J. Guan, L.-J. Xiao, *Tetrahedron* **2015**, 71, 7676-7680; c) M. R. Momeni, A. Brown, *J. Phys. Chem. A* **2016**, 120, 2550-2560; d) J. Tian, J. Zhou, Z. Shen, L. Ding, J.-S. Yu, H. Ju, *Chem. Sci.* **2015**, 6, 5969-5977; e) Y. Yan, J. Tian, F. Hu, X. Wang, Z. Shen, *RSC Adv.* **2016**, 6, 113991-113996.

[9] Q. Tang, W. Si, C. Huang, K. Ding, W. Huang, P. Chen, Q. Zhang, X. Dong, *J. Mater. Chem. B* **2017**, 5, 1566-1573.

[10] a) Y. Liu, N. Song, L. Chen, Z. Xie. *Dyes Pigments*

2017, 147, 241-245; b) L. Quan, S. Liu, T. Sun, X. Guan, W. Lin, Z. Xie, Y. Huang, Y. Wang, X. Jing. *ACS Appl. Mater. Interfaces*, **2014**, 6, 16166-16173.

[11] a) J. Ge, Q. Jia, W. Liu, L. Guo, Q. Liu, M. Lan, H. Zhang, X. Meng, P. Wang, Adv. Mater. **2015**, 27, 4169. b) W. Li, P. Rong, K. Yang, P. Huang, K. Sun, X. Chen, Biomaterials **2015**, 45, 18. c) J. Ge, Q. Jia, W. Liu, M. Lan, B. Zhou, L. Guo, H. Zhou, H. Zhang, Y. Wang, Y. Gu, X. Meng, P. Wang, Adv Healthc Mater **2016**, 5, 665-675.

10.1002/asia.201701727

WILEY-VCH

Entry for the Table of Contents (Please choose one layout)

Layout 1:

COMMUNICATION

Text for Table of Contents

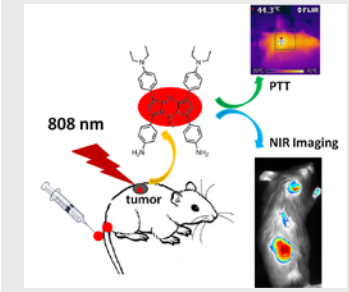

*Author(s), Corresponding Author(s)**

Page No. – Page No.

Title

Layout 2:

COMMUNICATION

((Insert TOC Graphic here))

*Author(s), Corresponding Author(s)**

Page No. – Page No.

Title

Text for Table of Contents